Microrheology and Characteristic Lengths in Wormlike Micelles made of a Zwitterionic Surfactant and SDS in Brine

Erick Sarmiento-Gomez, David Lopez-Diaz, and Rolando Castillo*

Instituto de Fisica, Universidad Nacional Autonoma de Mexico, P.O. Box 20-364, Mexico D. F. 01000

Received: May 31, 2010; Revised Manuscript Received: August 11, 2010

We study the Brownian motion of probe particles embedded in a wormlike micellar fluid made of a zwitterionic surfactant *N*-tetradecyl-*N*,*N*-dimethyl-3-ammonio-1-propanesulfonate (TDPS), sodium dodecyl sulfate (SDS), and salty water to get structural and dynamical information of the micellar network. The motion of the probe particles was tracked with diffusing wave spectroscopy, and the mean square displacement as a function of time for the particles was obtained. This allowed us to obtain the long-time diffusion coefficient for microspheres moving in the micellar network and the cage size where each particle is harmonically bound at short times in that network. The bulk mechanical susceptibility of the fluid determines the response of the probe particles excited by the thermal stochastic forces. As a consequence, the mean square displacement curves allowed us to calculate the elastic (storage) and the viscous (loss) moduli as a function of the frequency. From these curves, spanning a wide frequency range, we estimated the characteristic lengths as the mesh size, the entanglement length, the persistence length, and the contour length for micellar solutions of different zwitterionic surfactant concentration, surfactant ratio ([SDS]/[TDPS]), salt concentration, and temperature. Mesh size, entanglement length, and persistence length are almost insensitive to the change of these variables. In contrast, the contour length changes in an important way. The contour length becomes shorter as the temperature increases, and it presents a peak at a surfactant ratio of $\sim 0.50-0.55$. When salt is added to the solution, the contour length presents a peak at a salt concentration of ~ 0.225 M, and in some solutions, this length can reach values of ~ 12 μm. Scission energies help us to understand why the contour length first increases and then decreases when salt is added.

1. Introduction

In solution, amphiphilic molecules self-assemble to form various supramolecular structures, the geometry of which can be spherical, cylindrical, lamellar, etc. The preferred geometry is fixed by the spontaneous curvature determined by the most effective packing of the assembled aggregates. Therefore, the organization within these supramolecular structures will depend on a complex interplay of molecular geometry, amphiphilic character, and charge of all the involved molecules in the supramolecular structures. This interplay can be modified by many factors as surfactant concentration, added cosurfactants or hydrotope salts, as well as pH, temperature, and ionic strength of the media. The preferred interfacial curvature optimizes the system energetically but does not account for the effects of entropy. At low concentration, below the critical micelle concentration (CMC), entropy favors a uniform dissolution of the amphiphile in the solvent so that self-assembly and aggregation is negligible. Above the CMC, interaction dominates, and entropy effects are reduced. Consequently, the number of aggregates, usually spherical, sharply increases.

Cylindrical micelles are formed by amphiphiles with moderate spontaneous curvature. In these aggregates, energy is optimized when the curvature is uniform everywhere, forming long, linear structures (wormlike micelles, WMs). However, the system entropy introduces a degree of randomness through bending of the cylindrical micelles, which adds conformational entropy in a manner similar to the configurational entropy of polymeric chains and through topological defects, in the form of end caps, branch junction points, or a combination of both. These two defects are introduced by the formation of regions with differing local curvatures, but incurring in different energetic penalties. The overall entropic gain associated with end caps is greater than that of branch points. Although the appearance of topological defects introduces an entropy gain, the type of defect that dominates the system is set by the amphiphile spontaneous curvature. If the scission energy, E_{sc}, of a micelle (the energy required to create two end caps from an infinite cylinder) is large enough, then the semiflexible linear micelles can become very long and entangled at a relatively low total volume fraction of surfactant. The distance between entanglement points along a WM will be denoted by l_e. End caps increase entropy by increasing the number of micelles in a given system. Thus, lowering the scission energy shortens the total contour length, L_c, of the linear micelles. On the other hand, branch junction points increase the number of possible configurations, enabling percolation, and the formation of extended micellar networks, which leads to a multiconnected rather than an entangled network of cylindrical micelles. A review of junctions and end caps in self-assembled WMs can be found elsewhere.[1]

Transitions between linear and branched micelles are unusual. For nonionic surfactants in water, as the temperature increases, branched networks are formed, whereas linear micelles appear at lower temperatures.[2] This anomalous behavior apparently is due to the effect of temperature on the spontaneous curvature, rather than to the energy/translational entropy balance. In ionic surfactants, when salt is added, the electrostatic repulsions between head groups are screened, inducing a linear growth.

* To whom correspondence should be addressed. E-mail: rolandoc@fisica.unam.mx.

10.1021/jp104996h © 2010 American Chemical Society
Published on Web 09/08/2010

Atomistic molecular dynamics simulations have clearly shown this effect.[3] However, after a maximum, salt addition suggests a decrease in the micellar size. Nevertheless, for the case of long WMs in brine that exhibit an amazingly high fluidity that not can be accounted for by the reptation model, two mechanisms, not critically examined yet, have been proposed.[4−6] In these mechanisms, local stress relaxes instead of disentangling through a combination of reptation or breakage and recombination, as proposed in the Cates model,[7] it relaxes by sliding the cross-links along the micelles through the viscous flow on the surfactant molecules or by other processes that occur when the micellar tread collides with the network. They form transient cross-links that recombine on the other side of the encountered micelles (ghostlike crossing).

The study of structure, equilibrium behavior, and rheology of WMs has a long history, and it is examined in several review articles.[8−12] WMs have been investigated because their intriguing properties, such as the nonlinear rheological behavior with a plateau in the shear stress (σ) vs shear rate ($\dot{\gamma}$) flow curve wherein many cases shear banding is observed, their analogies with polyelectrolytes and polymers, and because WM solutions turned out to be important due to their applications[8] in fracture fluids, as drag-reducing agents, as templates in material technology, and in products of personal care, as well as in household products.

The response of a fluid with linear wormlike aggregates to mechanical perturbation is viscoelastic.[12] In the semidilute regime, where the surfactant concentration is between the overlap concentration and a concentration at which the network mesh size, ξ, is larger than the WM persistence length, l_p, the linear rheology is dominated in a good approximation by a single relaxation time at low frequencies, as in a Maxwellian fluid. Here, the stress relaxation function can be approximated by $G(t) = G_0 \exp(-t/\tau)$. G_0 denotes the elastic modulus, which is related to the micellar mesh size, and τ is the relaxation time.[8−12] The reptation-reaction model[7] for WMs proposes that τ is the geometric mean of two characteristic times: for micellar breaking and recombination, τ_b, and for micellar reptation, τ_R, where τ_b must be much smaller than τ_R. Therefore, the linear rheology at low frequencies in linear WMs is dominated by reptation and by reversible breaking and recombination between them.

The response of any material to shear excitations is characterized by the complex shear modulus $G^*(\omega)$ that determines the stress induced on a material upon application of an oscillatory shear strain, γ, at a frequency, ω. The real part of $G^*(\omega)$, the storage or elastic modulus $G'(\omega)$, is in phase with the applied shear strain. The imaginary part of $G^*(\omega)$, the viscous or loss component of the stress, $G''(\omega)$, is in phase with the shear rate, $\dot{\gamma}$. Regularly, $G^*(\omega)$ is usually determined by using mechanical rheometers in which viscoelastic properties are measured by application of strain while measuring stress or vice versa. However, in the past decade, microrheological techniques have successfully matured.[13−15] These techniques make use of micrometer-sized probe particles that are embedded into a fluid, usually complex, to locally measure the viscoelastic response of these complex fluids. The response can be measured either by actively manipulating the probe particles or by passively measuring the mean square displacement, $\langle \Delta \mathbf{r}^2(t) \rangle$, of them. The bulk mechanical susceptibility of the fluid determines the response of the probe particles excited by the thermal stochastic forces, which lead to Brownian motion. The measured $\langle \Delta \mathbf{r}^2(t) \rangle$ can be related to $G^*(\omega)$ by describing the motion of the particles with a generalized Langevin equation incorporating a memory function to take into account the viscoelasticity of the fluid.[16] In this way, the particle fluctuation spectrum can be used to measure the stress relaxation spectrum of the fluid. Here, in contrast to mechanical rheometers, there is no strain applied on the material during the measurement. This is particularly useful in complex fluids in which even small imposed strains can cause structural reorganization of the material and, consequently, a change in the viscoelastic properties. Various methods have been used to measure the displacement fluctuations of the embedded particles, such as video tracking[17−19] and diffusing wave spectroscopy (DWS).[20−22] In the latter, a dynamic light-scattering technique is used to measure the $\langle \Delta \mathbf{r}^2(t) \rangle$ of the probe particles.

DWS microrheology was used for the first time in WM solutions by van Zanten and Rufener.[23] They showed that the observed $\langle \Delta \mathbf{r}^2(t) \rangle$ of polystyrene microspheres embedded in water solution of WMs made of cetyltrimethylammonium bromide (CTAB) and KBr is well described by Brownian particles moving in a Maxwell fluid. The Maxwell fluid parameters were of the same order of magnitude as those obtained by mechanical rheology for similar systems. Cardinaux et al.[24] studied concentrated aqueous solutions of hexaethylene glycol mono *n*-hexadecyl ether that self-assembles in WMs at high surfactant concentration, using a combination of single- and multispeckle DWS with polystyrene microspheres of two diameters. They needed a factor of 1.52−2 of unknown origin to obtain a quantitative agreement between microrheology and classical rheometry. Bellour et al.[25] studied the aqueous solutions of hexane sulfonate cetyltrimethylammonium and heptane sulfonate cetyltrimethylammonium ($CTAC_7SO_3$). These authors obtained $\langle \Delta \mathbf{r}^2(t) \rangle$ curves for polystyrene particles embedded in the WM solution in the semidilute regime. They described these curves with an appropriate expression over 10 decades in time, during which three different regimes for the motion of the particles were recognized. They found good agreement between the rheological parameters measured with DWS and those measured with mechanical rheology. Galvan-Miyoshi et al.[26] studied WMs in a water solution of CTAB and sodium salicylate (NaSal), at different temperatures and CTAB/NaSal ratios. From the time evolution of the mean square displacement of particles, they could obtain $G'(\omega)$ and $G''(\omega)$ at high frequencies that allowed them to estimate the characteristic lengths of the WM network; namely, ξ, l_e, l_p, and L_c. Willenbacher et al.[27] studied a water solution of cetylpyridinium chloride (CPyCl) and NaSal at different temperatures. They found a quantitative agreement between mechanical high frequency rheometry and DWS, and they were able to find E_{sc}, ξ, and l_p for the WMs. These authors also studied in this system the linear-to-branched micelle transition.[28] They attributed the first viscosity maximum to a transition from linear to branched micelles, the second viscosity increase to a decrease of the branching density accompanied by an increase of L_c, and the second viscosity decrease to a shortening of the WMs with an increase in the branching density. Recently, Oeschlaeger et al.[29] investigated the variation of G_0, E_{sc}, and l_p in WMs formed by CTAB in the presence of different nonpenetrating counterions (Br^-, NO_3^-, and ClO_3^-), and compared their results with the WM system made of CPyCl and NaSal, in which the NaSal produces a penetrating counterion.[28]

WM solutions containing zwitterionic surfactants have received less attention than cationic surfactants, although important examples can be found in the literature, as the mixtures of alkyldimethylamineoxides with cationic and anionic surfactants,[30] or the water solutions of anionic and zwitterionic

surfactants involving betaines and sulfobetaines. Betaines have shown a strong synergism when mixed with sodium dodecyl sulfate (SDS), clearly exemplified by the CMC dependence on composition.[31] The mixture of SDS and lauryl amdidopropyl betaine has been systematically studied.[32] In sulfobetaines, where charge is not sensitive to pH, salt addition markedly favors the interaction between zwitterionic surfactants and SDS.[31] This is also the case for the SDS water solution of *N*-alkyl-*N*,*N*-dimethyl-3-ammonio-1-propanesulfonate zwitterionic surfactants, which have been studied for the case of three different alkyl tail lengths.[31] These mixtures behave nonideally with salt addition, although the studied salt concentration range (<0.1 M) was not large enough to produce WMs. Our group has recently reported,[33] however, that at higher salt concentrations, the water solution of SDS and *N*-tetradecyl-*N*,*N*-dimethyl-3-ammonio-1-propanesulfonate (TDPS) can form WMs in a particular region of its phase diagram, which is mostly unknown. The TDPS/SDS/brine system self-assembles into long and flexible cylindrical micelles for surfactant ratios of $0.43 < R < 0.65$ (R = [SDS]/[TDPS]) in brine at temperatures of $T \sim 20-70$ °C, and zwitterionic surfactant concentration $C_z \sim 2-47$ mM. The overlap concentration is $C^* \sim 7-8$ mM, as reported quite recently.[33]

For larger R values, there is some evidence of the existence of a lamellar phase ($R > 0.65$).[34] The main features of the rheological behavior of this system in the dilute regime have been reported.[33] The system presents a shear thickening transition. The critical shear rate increases as the zwitterionic concentration increases, and it follows the Arrhenius' law. A possible model for the WM structure has also been proposed.[34] The rheological behavior of this system in the semidilute regime has also been investigated using mechanical rheometry.[34] In a good approximation, it behaves Maxwell-like at low frequencies, because a single relaxation time dominates the linear viscoelastic regime. τ_b and τ_R have been estimated, as well as how they vary with surfactant ratio, temperature, and mainly with salt addition. In most of the cases, $\tau_b \ll \tau_R$. When this is not obeyed, the system deviates from the Maxwellian behavior. A master dynamic phase diagram for σ/G_0 vs $\dot{\gamma}\tau$, which is invariant with surfactant ratio and temperature, can summarize the nonlinear behavior for the system, when the WMs behave as neutral polymers. Flow curves for this system are composed of two stable branches corresponding to a high and to a low viscous fluid, separated by a stress plateau. Along this plateau, the fluid is inhomogeneous and presents gradient shear banding.[34]

The purpose of this paper is devoted to improving our understanding of the structure and the dynamical properties of the wormlike micellar fluid made of a zwitterionic surfactant TDPS, SDS, and salty water, by means of studying the Brownian motion of probe microspheres embedded in the fluid. The motion of the probe particles was tracked with DWS, and the $\langle \Delta \mathbf{r}^2(t) \rangle$ for the particles was obtained. This allowed us to obtain the long-time diffusion coefficient for microspheres moving in the WM network and the cage size where each particle is harmonically bound at short times in that network. $G'(\omega)$ and $G''(\omega)$ were calculated from the $\langle \Delta \mathbf{r}^2(t) \rangle$. From these curves, spanning a wide frequency range, we estimated the characteristic lengths of the WM network—namely, ξ, l_e, l_p, and L_c—for WM solutions with different zwitterionic surfactant concentrations; surfactant ratios, R; salt concentration; and temperature. As we will show below, ξ, l_e, and l_p are almost insensitive to the change of these variables. In contrast, L_c changes in an important way. L_c becomes shorter as the temperature increases, and it presents a peak at a surfactant ratio of $R \sim 0.50-0.55$. When salt is added to the solution, L_c presents a peak at a salt concentration of ~0.225 M, and in some solutions, this length can reach values of $L_c \sim 12$ μm. The way in which E_{sc} changes with salt addition helps us to understand why L_c first increases and then decreases when salt is added. In this study, we also make a comparison between the $G'(\omega)$ and $G''(\omega)$ coming from DWS and from mechanical rheometry.

2. Experimental Section

Materials. *N*-tetradecyl-*N*,*N*-dimethyl-3-ammonio-1-propanesulfonate (>99%) and sodium chloride (>99%) were from Sigma-Aldrich (USA). Sodium dodecyl sulfate (SDS, >99%) was from Merck (Germany). All the reagents were used as received. Water was Milli-Q water (nanopure-UV, USA; 18.3 MΩ). Microspheres of 800 nm and 2 μm were purchased from Bangs Laboratories Inc. (Fishers, IN). Weight concentration was obtained by gravimetric measurements prior total solvent evaporation.

Sample Preparation. All micellar solutions were prepared by weight. C_z denotes the zwitterionic surfactant concentration, and R, the surfactant ratio (R = [SDS]/[TDPS]). Because micellar solution viscosity is high at room temperature and to avoid colloidal agglomeration, we followed a two-step procedure to make the samples. In the first step, water, SDS, TDPS, and NaCl were mixed. Solutions were left for 24−48 h to relax. In the second step, the samples, placed in sealed cells to avoid water evaporation, were heated to 40 °C to reduce viscosity. Then, microspheres of 800 nm or 2 μm in water suspension (10%) were added while the samples were stirred. Stirring was maintained for 20 min, and subsequently, samples were sonicated for another 15 min to ensure a homogeneous dispersion. Samples were allowed to relax for 3 days at 30 °C in rectangular cuvettes of a thickness of $L = 2.5$ mm. To avoid interparticle interactions as well as hydrodynamic correlation, particle volume fractions were low, 0.0175 and 0.03 for microspheres of 0.8 μm and 2 μm, respectively. In some WM solutions, due to the small size of G_0, DWS measurements using 800 nm microspheres did not allow us to observe the linear regime at large times. Therefore, 2 μm microspheres were used to reach this linear regime in the $\langle \Delta \mathbf{r}^2(t) \rangle$ curves, taking advantage of the fact that the microrheological results do not depend on the size of the particles.[25,26] Anyway, we made some tests in some WM solutions with not so small G_0, using both microsphere sizes. We did not observe any difference in the viscoelastic moduli between both measurements within the experimental error.

Rhoelogy. Mechanical rheometric measurements were performed in a Bohlin Gemini HRnano rheometer (Malvern Instruments, UK). All dynamic viscoelastic spectra measurements were performed using a cone−plate geometry (4°−40 mm). Measurements were made at least two days after the solution preparation to allow them to reach equilibrium.

DWS. Our DWS setup is a homemade instrument described elsewhere.[26] DWS theory connects temporal field fluctuations of the scattered light emerging from a turbid suspension to the dynamics of the probe particles embedded in the suspension. That is, the $\langle \Delta \mathbf{r}^2(t) \rangle$ of the probe particles can be determined by collecting the scattered intensity from a single speckle over a sufficiently long collection period and evaluating the time-averaged intensity autocorrelation function (ACF), $g^{(2)}(\tau)$. The time averaged field ACF, $g^{(1)}(\tau) = \langle E(0)\ E^*(t) \rangle / \langle |E(0)|^2 \rangle$, is related to the measured $g^{(2)}(\tau)$ through the Siegert relation: $|g^{(2)}(\tau)| = 1 + \beta |g^{(1)}(\tau)|^2$, where β is an instrumental factor determined by the collection optics. When all the scattering particles suspended in the fluid are free to explore the same

local environment during the course of a measurement, the scattering process is ergodic, and time- and ensemble-averaged correlation functions are identical. In transmission, the liquid under investigation, with the scattering particles immersed in it, can be treated as a slab with an infinite transverse extent and a thickness $L \gg l^*$; here, l^* is the transport mean free path. In this case, the expression of the time averaged field ACF, $g^{(1)}(\tau)$ is[16]

$$g^{(1)}(t) = \frac{\frac{L/l^* + 4/3}{\alpha^* + 2/3}\left(\sinh[a^*x] + \frac{2}{3}x\cos[a^*x]\right)}{\left(1 + \frac{4}{9}x^2\right)\sinh\left[\frac{L}{l^*}x\right] + \frac{4}{3}x\cosh\left[\frac{L}{l^*}x\right]} \quad (1)$$

where $x = [k_0^2\langle\Delta r^2(t)\rangle]^{1/2}$ and $\alpha^* = z_0/l^*$. z_0 is the distance into the sample from the incident surface to the place where the diffuse source is located. If l^* is known in the sample, the $\langle\Delta\mathbf{r}^2(t)\rangle$ can be obtained by using eq 1. The ability to store energy upon deformation changes the temporal correlations of the stochastic forces acting on the particle at thermal equilibrium, since the suspending medium must satisfy the fluctuation dissipation theorem. If we assume that $\tilde{\eta} = \tilde{\zeta}/6\pi a$, where $\zeta(t)$ is the Maxwellian fluid time-dependent memory function that accounts for both energy loss and storage upon deformation, s is the frequency in the Laplace domain, and a is the particle radius, the relation between $\tilde{G}(s)$ and $\langle\Delta r_2(t)\rangle$ can be written, neglecting the inertial terms, as[16]

$$\tilde{G}(s) = \frac{s}{6\pi a}\left[\frac{6k_BT}{s^2\langle\Delta\tilde{\mathbf{r}}^2(s)\rangle}\right] \quad (2)$$

Here, k_B is the Boltzmann's constant. Using the unilateral Fourier transform, an expression for the viscoelastic modulus as a function of frequency can be written as[16]

$$G^*(\omega) = G'(\omega) + iG''(\omega) = \frac{k_BT}{\pi a i\omega F_u[\langle\Delta\mathbf{r}^2(t)\rangle](\omega)} \quad (3)$$

Several procedures have been followed by different authors[16,23,35] to determine F_u. In our case, numerical inversion of eq 1 allowed us to obtain $\langle\Delta\mathbf{r}^2(t)\rangle$. Instead of making any transformation to the $\langle\Delta\mathbf{r}^2(t)\rangle$ curve, we first fitted the curve to a model curve proposed by Bellour et al.[25] for describing the $\langle\Delta\mathbf{r}^2(t)\rangle$ of the colloidal particles in Brownian motion embedded in a WM solution, over several decades in time. The model curve is given by

$$\langle\Delta\mathbf{r}^2(t)\rangle = 6\delta^2\left(1 - e^{-\left(\frac{D_0}{\delta^2}t\right)^{\alpha}}\right)^{1/\alpha}\left(1 + \frac{D_m}{\delta^2}t\right) \quad (4)$$

Here, $6\delta^2$ is the value of $\langle\Delta\mathbf{r}^2(t)\rangle$ at the plateau, D_0 is the diffusion coefficient for particles in the solvent at infinite dilution, and D_m is the diffusion coefficient for the particles for long times. To obtain the real and complex components of $G^*(\omega)$, we calculated the Laplace transform of the computed fitting curve and after transforming $s \rightarrow i\omega$ (analytic continuity), we introduced it into eq 2 to get eq 3.

Multispeckle DWS in transmission geometry was used to ensure that the sampling was ergodic. Our multispeckle DWS in transmission geometry setup is described elsewhere.[26] Time overlap between DWS and multispeckle DWS is around 4 orders of magnitude, and measurement times were about 3600 s.

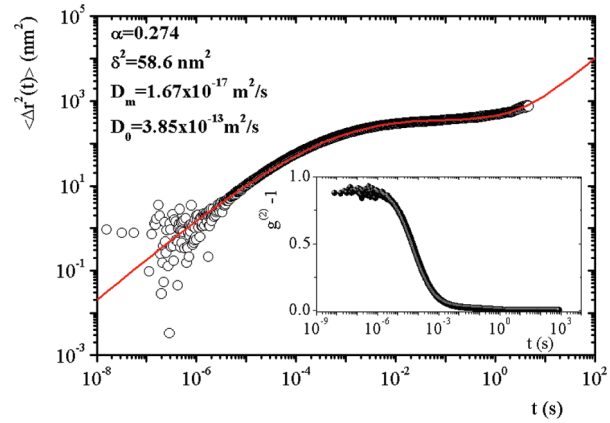

Figure 1. A typical $\langle\Delta\mathbf{r}^2(t)\rangle$ curve obtained in a DWS experiment for WM solutions of the system TDPS/SDS/brine (C_z = 46 mM, [NaCl] = 0.5M, R = 0.45, and T = 25 °C) using microspheres of a diameter of 800 nm at a volume fraction of 0.0175. The inset corresponds to the intensity time correlation function for the same solution.

Finally, l^* was obtained from transmittance and reflectance measurements of the samples to be investigated using an integrating sphere. This method is described elsewhere.[36] Just to assess the quality of our l^* measurements for colloidal suspensions of particles with different sizes and particle volume fractions, we calculated l^* using Mie scattering theory following the procedures developed by several authors.[37−39] The agreement between l^* measured using the method employing the integrating sphere and l^* calculated with Mie scattering theory is excellent. There is just a 3.8% mean deviation between theory and experiment. Other tests can be found elsewhere.[36]

3. Results and Discussion

Figure 1 shows a typical $\langle\Delta\mathbf{r}^2(t)\rangle$ curve measured for 800 nm diameter microspheres dispersed in a WM solution spanning over more than 7 orders of magnitude in time. In this particular case, C_z = 46 mM, R = 0.45, [NaCl] = 0.5 M, and T = 25 °C. The $\langle\Delta\mathbf{r}^2(t)\rangle$ curve is the result of a numerical inversion of eq 1, in which $g^{(1)}(\tau)$ came from a DWS experiment (inset in Figure 1). Afterward, the $\langle\Delta\mathbf{r}^2(t)\rangle$ was fitted to the model proposed by Bellour et al.,[25] as described in the Experimental Section, leaving δ, D_m, D_0, and α as free parameters. We observe in this figure three different regimes of motion, which apparently are shared by all micellar solutions reported in the literature.[24−26] At short times, there is a regime in which $\langle\Delta\mathbf{r}^2(t)\rangle$ is almost a linear function of time; $\langle\Delta\mathbf{r}^2(t)\rangle = 6D_0t$, where D_0 is the local diffusion coefficient. At intermediate times, $\langle\Delta\mathbf{r}^2(t)\rangle$ remains constant for a given time interval (a plateau). Here, the model[25] is built to describe the motion of Brownian particles harmonically bound around a stationary mean position. As a consequence, $\langle\Delta r^2(t)\rangle = 6\delta^2(1 - e^{-(D_0/\delta^2)t})$, where the particle's amplitude of the motion, the cage size δ, is related to the elastic modulus, G_0 ($\delta^2 = k_BT/[6\pi aG_0]$), which does not depend on ω; this result can be obtained by substituting this particular $\langle\Delta\mathbf{r}^2(t)\rangle$ in eq 2. At these intermediate times, particles are bound to their mean position, on time scales smaller than the longest characteristic time of the micellar system, $\tau_M = \eta_m/G_0$;[7] here, η_m is the long-time viscosity of the system. At the inflection point, $6\delta^2$ is the value of the mean square displacement. In a WM fluid, the cage where particles are momentarily trapped fluctuates due to the breaking/reptation process. Then, at longer times, $\langle\Delta\mathbf{r}^2(t)\rangle$ is

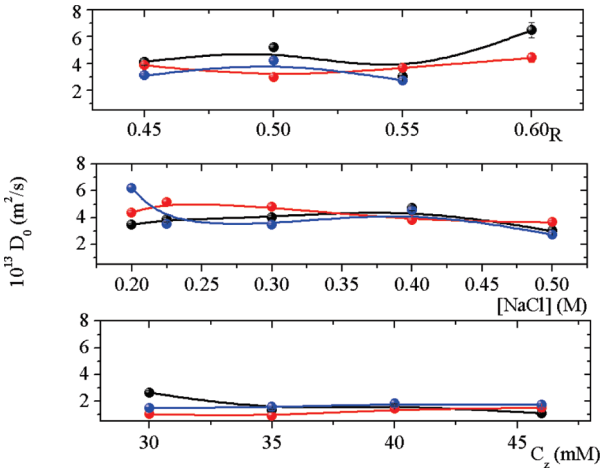

Figure 2. Short time local diffusion coefficient for microspheres as a function of R, added salt, and zwitterionic concentration, at different temperatures: 20 (black), 25 (red), and 30 °C (blue). Upper panel: C_z = 46 mM, [NaCl] = 0.5 M, and microsphere diameter = 800 nm. Middle panel: C_z = 46 mM, R = 0.55, and microsphere diameter = 800 nm. Lower panel: R = 0.55, [NaCl] = 0.225 M, and microsphere diameter = 2 μm. Lines are just a guide to the eye.

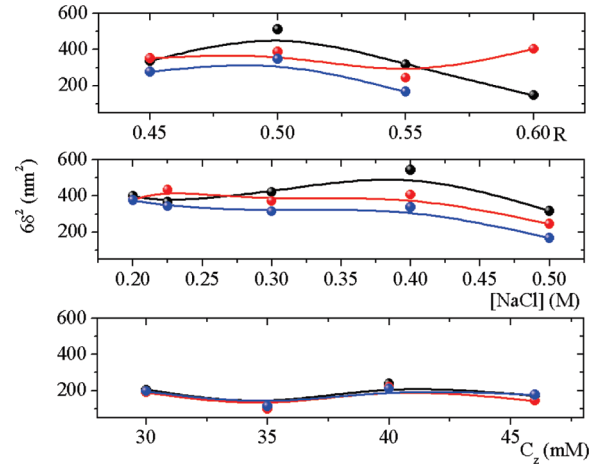

Figure 3. The mean square displacement at the inflection point, where particles are momentarily trapped in a cage at intermediate times, for microspheres as a function of R, added salt, and zwitterionic concentration, at different temperatures: 20 (black), 25 (red), and 30 °C (blue). Upper panel: C_z = 46 mM, [NaCl] = 0.5 M, and microsphere diameter = 800 nm. Middle panel: C_z = 46 mM, R = 0.55, and microsphere diameter = 800 nm. Lower panel: R = 0.55, [NaCl] = 0.225 M, and microsphere diameter = 2 μm. Lines are just a guide to the eye.

again a linear function of time, $\langle \Delta \mathbf{r}^2(t) \rangle = 6D_m t$. As a consequence, it was proposed that $\langle \Delta \mathbf{r}^2(t) \rangle = 6\delta^2(1 - e^{-(D_0/\delta^2)t})(1 + (D_m/\delta^2)t)$.[25] However, this last expression did not describe correctly the dynamics at the plateau onset time because dynamics of the microspheres exhibits a very broad time relaxation spectrum. This led to include the parameter α to give eq 4.[25] These three regimes are present in all the micellar solutions when WMs are present, no mater the R value or the temperature.

Figures 2, 3, and 4 summarize the values for the fitting parameters D_0, δ, and D_m for the $\langle \Delta \mathbf{r}^2(t) \rangle$ curves of microspheres dispersed in different WM solutions, where R values, the added salt, the zwitterionic concentration, and temperature were varied. As observed in Figure 2, D_0 is not importantly affected when concentration or temperature is varied. The microsphere diffusion at short times must be close to the value of diffusion of microspheres in brine. It is not practical to make an independent

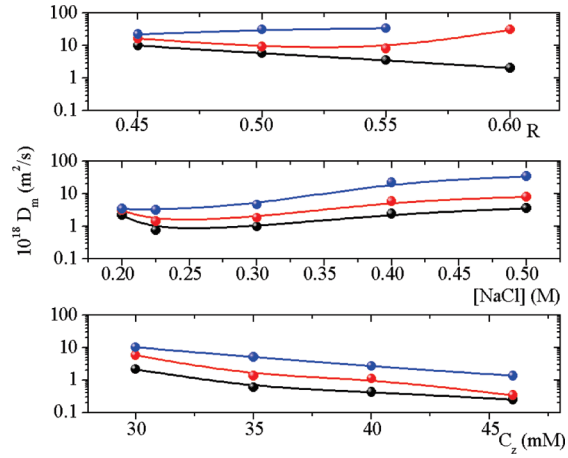

Figure 4. Long time diffusion coefficient for the microspheres as a function of R, added salt, and zwitterionic concentration, at different temperatures: 20 (black), 25 (red), and 30 °C (blue). Upper panel: C_z = 46 mM, [NaCl] = 0.5 M, and microsphere diameter = 800 nm. Middle panel: C_z = 46 mM, R = 0.55, and microsphere diameter = 800 nm. Lower panel: R = 0.55, [NaCl] = 0.225 M, and microsphere diameter = 2 μm. Lines are just a guide to the eye.

measurement of D_0 for microspheres in brine to test these numbers without avoiding particle flocculation, because the quantity of added salt is important. However, the measured values are relatively close to the values of D_0 for microspheres in plain water at 25 °C; namely, for 800 nm microspheres $D_0 = 5.5 \times 10^{-13}$ m^2/s, and for 2 μm microspheres, $D_0 = 2.1 \times 10^{-13}$ m^2/s.

Figure 3 gives an estimation of the mean square displacement of the microspheres in the cage; we preferred to present $6\delta^2$ values because they are more useful for interpretation. Clearly, the cage where particles are momentarily trapped is larger for the smaller particles. The cage size is usually larger at lower temperatures. $6\delta^2$ does not change considerably with R, although there is a small maxima at R = 0.5. It is also almost invariant with salt addition, although at high salt concentrations, a small decrease in δ can be observed. This could be indicating that at high salt concentrations, electrostatic interactions are completely screened, and the network might be more folded and shrunk. The zwitterionic concentration does not seem to have any appreciable effect on $6\delta^2$. In comparison, the average value of $6\delta^2$ in WM networks of other systems is smaller. To be exact, for CTAB/NaSal,[26] $6\delta^2 \sim 52$ nm^2 and for $CTAC_7SO_3$, $6\delta^2 \sim 51$ nm^2.[25] This will introduce profound differences in behavior between those systems and the system of interest here, since δ is related to G_0. As we will see below, G_0 is much smaller in the TDPS/SDS than in the other two mentioned systems (for CTAB/NaSal, G_0 = 63 Pa at 100 mM in both components, and for $CTAC_7SO_3$, G_0 = 19 Pa at a surfactant concentration of 2%).

In Figure 4, the diffusion coefficient for long times for the 800 nm and the 2 μm microspheres in the WM solutions are presented. D_m is dominated by the long-time viscosity of the mixture η_m through $D_m = k_B T/6\pi a\eta_m$. As the temperature increases, D_m also increases because η_m decreases with temperature following an Arrhenius behavior.[40] In the same way, for a given temperature, D_m decreases as C_z increases because η_m increases as C_z increases. D_m does not change appreciably when varying the R value, although it increases as salt is added to the WM solution.

The dynamics of the microspheres at the plateau onset time shows a broad relaxation spectrum, revealed by the values for

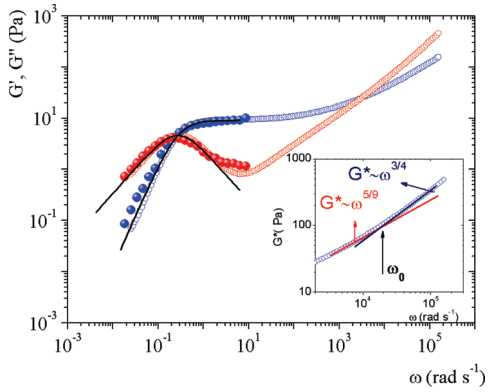

Figure 5. Viscoelastic spectra for the same solution shown in Figure 1. Empty and filled points correspond to data obtained by using DWS and by using mechanical rheometry, respectively. Lines represent the best fit to a Maxwell fluid. The inset shows $G^* \sim \omega^{\nu}$ at high frequencies, where ν changes from 5/9 to 3/4.

the α parameter; the average value for α in the WM solutions is $\alpha = 0.31 \pm 0.03$. The smaller the α, the larger the relaxation spectra ($\alpha = 1$ indicates monoexponential relaxation). On average, our α values are slightly larger than the α values for WM solutions of CTAB/NaSal ($\alpha \sim 0.23-0.26$)[26] and of $CTAC_7SO_3$ ($\alpha = 0.25-0.30$).[25]

The viscoelastic spectra for the WM solutions were obtained, applying a Laplace transform and making $s \rightarrow i\omega$, as explained in the Experimental Section, to the curves producing the best fits to the Bellour et al.[25] model for the $\langle \Delta \mathbf{r}^2(t) \rangle$ experimental curves. An example of the elastic and viscous moduli as a function of the frequency obtained by using this procedure is presented in Figure 5, where the elastic (real part) and the viscous (imaginary part) components of G^* are shown. The same kind of data obtained with a mechanical rheometer at low and intermediate frequencies is also presented. The agreement between the moduli obtained by DWS and by mechanical rheometry at low and intermediate frequencies is quite good. At low frequencies, the behavior of the fluid is Maxwellian. Here, stress relaxation occurs mainly through micellar reptation and by micellar breaking and recombination. A single relaxation time dominates. The plateau modulus and the relaxation time were obtained from the first crossover. In the particular case of Figure 5, the solid lines correspond to the best fit to a Maxwell fluid, which corresponds to $G_0 = 8.89$ Pa and $\tau = 4.1$ s. DWS microrheology reaches a bandwidth far beyond the conventional rheometry, allowing us to observe two crossovers in G^*, as presented in Figure 5. Probe size and solvent inertial effects are negligible up to frequencies of $\omega > 10^5$ rad/s. At high frequencies, where time scales are shorter than those of WM breakage time, the Maxwellian stress relaxation processes are essentially frozen, and the micelles can be regarded as semiflexible chains. Stress relaxes via intramicellar processes: First, it is dominated by the Rouse−Zimm modes and then by the internal relaxation of individual Kuhn segments. In this frequency range, G^* exhibits a power law behavior, $G^* \sim \omega^{\nu}$, with the exponent $\nu \sim 5/9$ in the Rouse−Zimm regime that changes to $\nu \sim 3/4$, where internal bending modes of Kuhn segments dominate.[27] This change occurs at a critical frequency, ω_0, corresponding to the shortest relaxation time in the Rouse−Zimm spectrum. One important feature to be pointed out is related to the local minimum of $G''(\omega)$ after the first crossing between $G'(\omega)$ and $G''(\omega)$, denoted by $G''_{\min}$. This is usually better defined in DWS microrheology than in mechanical rheometry. This will be important for estimating the characteristic lengths of the WMs in solution, as shown below.

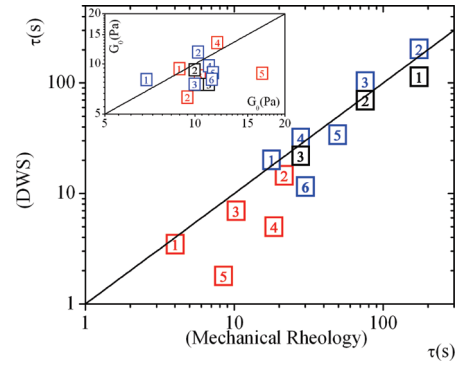

Figure 6. Comparison between DWS and mechanical rheometry measurements. Main figure for τ and inset for G_0. Experiments varying R (red squares) at $C_z = 46$ mM and [NaCl] = 0.5: **1**, $R = 0.45$, $T = 25$; **2**, $R = 0.5$, $T = 20$; **3**, $R = 0.5$, $T = 25$; **4**, $R = 0.55$, $T = 25$; **5**, $R = 0.6$, $T = 25$. Experiments varying [NaCl] (blue squares) at $C_z = 46$ mM, $R = 0.55$: **1**, [NaCl] = 0.2 and $T = 25$; **2**, [NaCl] = 0.225, $T = 20$; **3**, [NaCl] = 0.225, $T = 25$; **4**, [NaCl] = 0.225, $T = 30$; **5**, [NaCl] = 0.3 M, $T = 25$; **6**, [NaCl] = 0.4 M, $T = 25$. Experiments varying T (black squares) at $C_z = 46$ mM, $R = 0.45$, and [NaCl] = 0.5: **1**, $T = 20$; **2**, $T = 25$; **3**, $T = 30$. T in °C and [NaCl] is molar concentration.

Figure 6 presents measurements for G_0 and τ made with DWS vs measurements for G_0 and τ made with mechanical rheometry. The line with a slope of 1 would correspond to perfect agreement. On the average, the difference between our DWS measurements with respect to mechanical rheometry is ∼20% for G_0, and ∼35% for τ. In a general way, the values for G_0 and τ are always lower when measured with DWS than when measured with mechanical rheometry. The agreement between the measurements is good, although it is not excellent. The comparison of rheological data obtained by different methods is not an easy task because protocols play a central role. In particular, in mechanical rheology, cell geometry, cell parameters, sample preparation, and even different reactive stocks have been described as factors that could introduce deviations in WM rheology. In general, in mechanical rheology, it is not strange that measurements for different nominally identical samples have an error bar of ∼20% for G_0 and of ∼5% for τ. In DWS microrheology, it is usual for a WM sample measured in different days to has an error bar of ∼7% for G_0 and ∼8% for τ. Therefore, DWS microrheology seems to share some kind of these problems (sample preparation, probe particle dispersion method, etc.), so this has to be considered when DWS microrheology and mechanical rheology are compared. There are several factors that have been mentioned in the literature that could explain this difference, but none of them is completely satisfactory. It has been suggested that hydrotope salt ions in solutions could be responsible for this deviation,[26] but this suggestion was not supported by later experimental work.[28] Therefore, we do not expect that a small increase in SDS concentration is responsible for that behavior. However, it is important to note that the samples that present more deviation are those corresponding to higher R values, where the system is relatively close to a phase transition. Local structure formation or surfactant adsorption hindering the tracer motion could be a possible scenario, which could modify the parameters obtained with DWS. Another possibility could be that during sample preparation, the solution could reach the lamellar phase. As explained in the Experimental Section, samples have to be heated to 40 °C to reduce viscosity to introduce the microspheres in solution. Then, despite the waiting time employed and the heat treatment to go back to the WM phase, equilibrium might

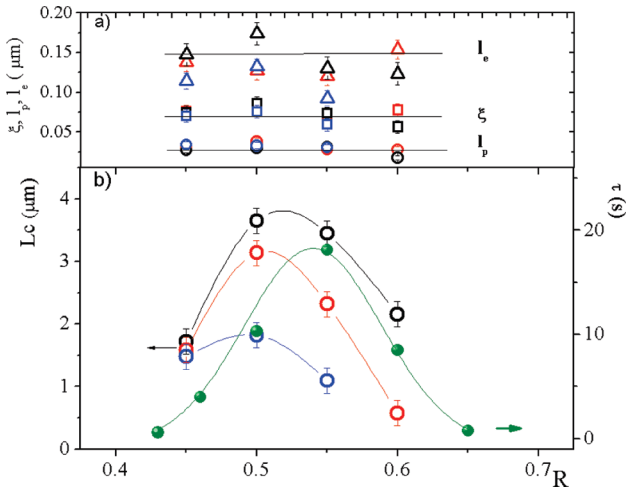

Figure 7. Characteristic lengths for WM solutions with different R and T (20 (black), 25 (red), and 30 °C (blue)), $C_z = 46$ mM, [NaCl] = 0.5 M. (a) ξ, l_p, l_e. (b) L_c. Relaxation times at 25 °C have been included (green solid points) for comparison. Lines are just a guide to the eye.

not be reached when the measurement was taken. Tracer sedimentation could be another possibility, but l^* measurements were quite constant during the time the samples were tested, as observed by other authors.[28] Aggregation of tracer particles has been mentioned with some evidence.[28] Our samples were revised after our measurement by optical microscopy, and aggregation was never observed. Particle size apparently is not influencing our measurement, in agreement with other researchers,[25] although for other systems, particle size has some influence.[28] This issue requires additional experimental work to be fully understood.

With the $G^*(\omega)$ obtained with DWS, it is possible to estimate the most important characteristic lengths of the WM network of the system, using approximate relations coming from theory. It is important to mention that theory developed for WMs is far from being complete; anyway, it could be of help to obtain approximate structural information about the WM network. As mentioned before, we are interested in how the WM characteristic lengths, ξ, l_p, l_e, and L_c, change when C_z, R, T, and the added salt are modified. The mesh size can be calculated by[41] $\xi = (k_BT/G_0)^{1/3}$. The persistence length of the WMs can be obtained directly from[27] $\omega_0 \approx k_BT/8\eta_m l_p^3$. The contour length of the WMs, L_c, can be obtained from the equation $G''_{min}/G_0 \approx l_e/L_c$, as given by Granek and Cates.[42] It is important to note that G''_{min}/G_0 is much less than 0.1 for most of our micellar solutions; therefore, this ratio produces relatively good values for l_e/L_c. l_e can be computed using[42] $l_e = \xi^{5/3}/l_p^{2/3}$.

In Figure 7, the effect of the surfactant ratio, R, on the characteristic lengths at different temperatures is presented for several WM solutions in which $C_z = 46$ mM, and [NaCl] = 0.5 M are maintained constant. l_e, ξ, and l_p are almost insensitive to changes in the surfactant ratio and temperature (Figure 7a). The values found in our system are $l_p \sim 35 \pm 5$ nm, which are not far from the l_p values obtained by other authors for WMs in different systems. In particular, for CTAB/NaSal/water at different NaSal/CTAB ratios, there are reports of $l_p \sim 23.5-25.1$ nm obtained with stress optic coefficient measurements,[43] and of $l_p \sim 36-40$ nm with small angle neutron scattering in the dilute regime.[12] In a recent study, modifying temperature and the NaSal/CTAB ratio, Galvan-Miyoshi et al. using DWS,[26] found values for l_p ranged from ~29 to 45 nm. In the system CPyCl (100 mM)/NaSal (60 mM), $l_p \sim 31-34$ nm using DWS[27] when $20 \le T \le 40$ °C. In the same system, l_p ranges from 26 to 30 nm as the NaCl/CPyCl concentration ratio varies from ~0.5 to 4 (CPyCl 100 mM).[28] The mesh size in our micellar solutions, $\xi \sim 75$ nm, is larger than in other systems. In the case of CTAB/NaSal/water, Galvan-Miyoshi et al. [26] obtained a size of $\xi \sim 35-45$ nm using DWS and $\xi \sim 39-53$ nm using mechanical rheometry, at different temperatures and NaSal/CTAB ratios; Nettesheim and Wagner[43] obtained $\xi \sim 40$ nm for a NaSal/CTAB ratio = 2; and Shikata et al.[44] found $\xi \sim 45$ nm for a ratio of 1.5 and 2, at 25 °C. WMs in water solution, formed by CTAB in the presence of different nonpenetrating counterions (Br^-, NO_3^-, and ClO_3^-), present ξ values around 22−30 nm obtained with DWS. [29] WMs in water solution of trimethylammonium tosylate and sodium dodecyl benzyl sulfonate, with a hydrotope salt or with added salt, present a size on the order of $\xi \sim 50-200$ nm (added salt) and $\xi \sim 100$ nm (hydrotope salt) using results coming from mechanical rheometry.[45]

It is important to note that there is a slight decrease in ξ for $R > 0.55$, which would be related to an increase in G_0.[34] This additional contribution to the elasticity could correspond to the onset of a transition to a multiconnected rather than an entangled network of cylindrical micelles. We will come back to this issue below. The entanglement lengths in the system of interest here are in the range of $l_e \sim 150$ nm, which is bigger than the values reported for WMs in a water solution of CTAB and NaSal at different ratios of these compounds and temperatures (l_e, ~ 40−75 nm).[26] In WMs of CTAB in the presence of different nonpenetrating counterions (Br^-, NO_3^-, and ClO_3^-) $l_e \sim 18-30$ nm. [29] The results just mentioned were obtained with DWS in both cases. With mechanical rheometry, WMs in a water solution of trimethylammonium tosylate and sodium dodecyl benzyl sulfonate produce a l_e in the range of $l_e \sim 80-700$ nm, depending on whether the added salt is penetrating or not.[45]

The effect of varying R and T on the L_c is presented in Figure 7b. A first feature to be observed in this figure is that L_c decreases as T increases. The entropic contribution induces smaller micelles as mentioned in the Introduction. A second feature is the maximum in L_c that appears in the range of $0.50 < R < 0.55$ for all temperatures. For comparison, we also included in this figure τ vs R, at 25 °C. The curve for τ obtained by mechanical rheology[34] presents a peak around $R = 0.55$, very close to the maxima presented by L_c. Both variables L_c and τ follow the same trend as R is varied. The maxima do not perfectly coincide. However, it is important to note that the curves in this figure are guides to the eye; therefore, there is an experimental uncertainty of where the maximum is in each curve. At constant surfactant volume fraction, φ, large τ values imply large WM contour lengths, L_c.[7,46] τ values for the system under study could be very large (ranging from ~5 to ~800 s, depending on R and the brine concentration[34]) when compared with the τ values obtained for the CTAB/NaSal system (~1−5 s),[47] as well as for other systems; namely, catanionic mixtures (~0.1−100 s),[48] zwitterionic and ionic surfactants mixtures (~1.5−15 μs),[30] and nonionic fluorocarbon surfactant mixtures (~0.02−2 s).[49] The effect of penetrating and nonpenetrating counterions on τ has been investigated by Oelschlaeger et al.[29] In the case of $T = 30$ °C, we do not present more data for $R > 0.55$ because apparently, as mentioned above, the solution is close to a transition to a lamellar phase, and there is a small decrease in ξ for $R > 0.55$ that could be an indication of the onset of a transition to a multiconnected network of cylindrical micelles. A signature of the structure could be provided by the exponent of a power law that relates the zero-shear viscosity to

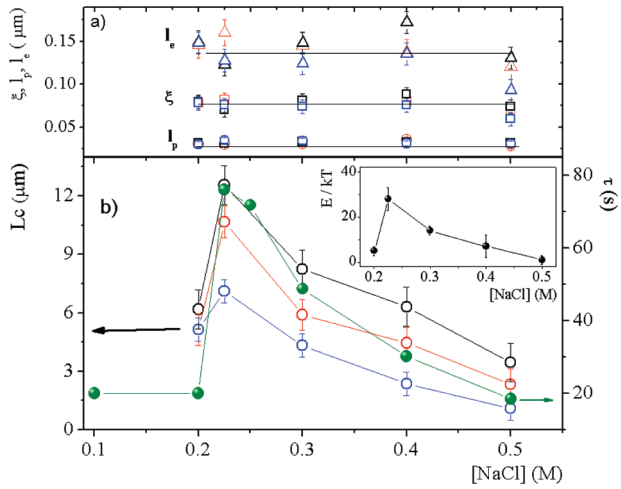

Figure 8. Characteristic lengths as a function of brine concentration in WM solutions with $R = 0.55$, $C_z = 46$ mM and different temperatures: 20 (black), 25 (red), and 30 °C (blue). (a) l_p, ξ, and l_e vs [NaCl]. (b) L_c vs [NaCl]. Here, τ vs [NaCl] at 25 °C has been included for comparison (green solid points). The inset in b represents the end cap energies as a function of the added salt. In all cases, the lines are guides to the eye.

volume concentration in the semidilute regime. For linear micelles, the Cates model[7] predicts a scaling behavior $\eta_0 \sim C_z^{\sim 3.5}$ (transforming into our notation). For a system consisting of linear and branched micelles, Cates's approach modified by the Lequeux model of reptation of branched micelles predicts an exponent between 2.4 and 3.5.[50] Power law exponents less than 2.4 cannot be accounted for by a reptation model. It has been suggested that such small values could indicate a mechanism of sliding connections in a saturated network.[4] We explored this issue. In our case, the exponent for $R = 0.45$ and $R = 0.55$ is ~3.6 and for $R = 0.60$ is ~1.9. So this means that at this thermodynamic state, the system is close to a transition, although the details are not understood. The WM length, L_c, for the TDPS/SDS/water system is larger than L_c for other reported systems. In WMs of CTAB/NaSal,[26] $L_c \sim 0.4-4.8$ μm, depending on the ratio of CTAB/NaSal and temperature. In WMs of CPyCl/NaSal, $L_c \sim 0.150-2.5$, μm depending on the CPyCl/NaSal ratio,[28] and $L_c \sim 0.070-0.3$ μm for nonpenetrating added salts. In the latter system, there is a complication because this size could be the length between branching points.[29]

Ionic strength of the fluid where WM are embedded is critical in determining growth, flexibility, and entangling. In a previous work,[34] it was already noticed that brine concentration has an important influence on the relaxation time of this WM system. Figure 8 presents our calculations for l_p, ξ, l_e, and L_c as a function of the added salt for different temperatures for WM solutions at $R = 0.55$ and $C_z = 46$ mM. l_p, ξ, and l_e are presented in Figure 8a. The R value used in this figure corresponds approximately to the maximum for both the relaxation time and the contour length in Figure 7. Surprisingly, there is no significant variation in these quantities as the salt concentration is varied. Likewise, temperature does not alter these WM lengths in an important way; only l_e presents a slight decrease as the temperature increases. The effect of added salt on L_c at different temperatures is presented in Figure 8b. Here, L_c is shorter as the temperature increases for the same quantity of added salt, revealing an increase in the entropic contribution, as mentioned in the Introduction. Nevertheless, the behavior of L_c with added salt is outstanding. At low salt concentrations, the contour size of the micelles is close to 5 μm. As the added salt reaches a value of 0.225 M, L_c jumps up to very large lengths (~12 μm at 20 °C). Addition of more salt results in a smooth decrease in the contour length of the WMs. Apparently, the addition of salt has an effect similar to adding SDS. In Figure 8b, also we have included how τ varies with salt addition at 25 °C; these τ values come from mechanical rheometry.[34] Both L_c and τ follow the same trend with added salt because at a constant surfactant volume fraction, φ, large τ values imply large WM contour lengths ($\tau \sim L_C\varphi^{3/4}$).[7,46] As mentioned in the Introduction, L_c is determined by a balance between the scission energy required to create two end caps and the entropy of mixing.[51−53] For charged micelles $E_{sc} = E_c - E_e$, where E_c is the end cap energy that promotes the micellar growth,[46] and $E_e \sim k_B T l_B R_{cs} \nu \varphi$ is the electrostatic contribution of the surface charges that favors the end caps over the cylindrical regions. Here, l_B is the Bjerrum length, R_{cs} is the cross section radius, and ν is the effective WM charge per unit length. At low salt concentrations ([NaCl] < 0.22, in Figure 8b), E_e probably is not vanishing, and the system presents a L_c according to the mentioned balance. However, the enlargement in the contour length observed when salt is added must be due to an increase in the E_{sc}. As the WMs are screened, the scission energy increases, because E_e vanishes as ν goes to zero. When an optimal salt concentration is reached ([NaCl] ~ 0.225 M), all electrostatic repulsions have been totally canceled, and the micellar network behaves as a neutral (living) polymer in which a maximum in contour length is reached: 12 μm in the solution with [NaCl] ~ 0.225 M at 20 °C. To confirm this issue, the E_{sc} of the WM were calculated from charts of L_c as a function of $1/T$, by using the expression $G''_{min}/G_0 \sim l_e/L_c \sim \exp(-E_{sc}/2k_BT)$. We present E_{sc} vs [NaCl] in the inset of Figure 8b. The scission energy shows the same tendency as τ and L_c when salt is added. The increase in E_{sc} (from 5 to 28 kT) promotes the micellar growth, and when E_{sc} declines as a consequence, micelles shorten. Similar results for E_{sc} have been found for water solutions of CPyCl, with a penetrating counterion as the sodium salicilate.[28] Nevertheless, E_{sc} is independent of the salt concentration when the added salt is a nonpenetrating salt; namely, $NaClO_3$, $NaNO_3$, or KBr.[29] We cannot discard that after the maxima of Figure 8b, other mechanisms are working in the micellar solution, as in other systems, forming extremely long WMs in brine that exhibit an amazingly high fluidity, which cannot be accounted by the reptation model. For these systems, there is an explanation based on assuming that local stress could relax by two other mechanisms, as mentioned in the Introduction.[3−5] The first mechanism is related to the relaxation by sliding the cross-links along the micelles through the viscous flow on the surfactant molecules. The second mechanism is related to the transient character of cross-links (ghostlike crossing). In our case, apparently the trend of E_{sc} points out that τ and L_c decrease because the WMs get shorter as salt is added. Future studies using freeze fracture on the WM solution could be of help to determine if these WM are prone to form branched micelles.

The effect of the zwitterionic concentration on characteristic lengths has been studied in the WM solutions with $R = 0.55$, $C_z = 46$ mM, [NaCl] = 0.225 M. This brine concentration corresponds to the maxima in L_c of Figure 8b; that is, where the WMs are totally screened by the addition of salt, and the WMs behave as neutral polymers. It is difficult to do a quantitative analysis of these results because the ionic strength is not exactly the same in all of the solutions. As the TDPS concentration increases, the SDS concentration also increases, although the R value is maintained constant. Nevertheless, qualitative results can be obtained. In Figure 9, the WM characteristic lengths vs C_z are presented. l_e fluctuates as C_z

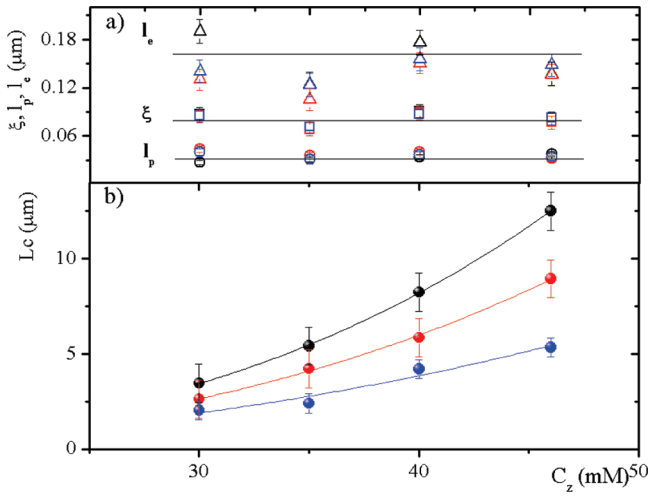

Figure 9. Characteristic lengths as a function of the zwitterionic concentration (C_z) at $R = 0.55$, when WMs are totally screened ([NaCl] = 0.225 M), at three different temperatures: 20 (black), 25 (red), and 30 °C (blue). Lines are the best fit to a power law.

increases and does not present a defined trend. ξ is almost a constant as C_z is varied. According to polymer theory, contour length must grow as $L_c \sim C_z^{\beta}$, where β is must be around $\sim 0.5-0.6$.[6,54] In Figure 9b, we observe that L_c follows this kind of law, but with a different exponent. The exponents are in the range $\beta \sim 2.47-3.05$, depending on the temperature. Other authors have also found large discrepancies, as in the case of $C_{16}E_6/D_2O$ where $\beta = 1.2$.[55] This indicates that the concentration dependence of the contour length is an issue that requires additional experimental and theoretical work to be explained.

4. Concluding Remarks

From this study, we know that in a restricted range of concentrations, the WM micellar fluid, made of a zwitterionic surfactant *N*-tetradecyl-*N*,*N*-dimethyl-3-ammonio-1-propanesulfonate (TDPS), sodium dodecyl sulfate (SDS), and salty water, forms WMs of known characteristic lengths. Using diffusing wave spectroscopy to track the motion of particles embedded in this fluid, we obtained the mean square displacement of these Brownian particles in the WM network. We were able to determine the size of the cage where each particle is harmonically bound at short times, the long-time diffusion coefficient, and experimental values for the exponent that accounts for the broad spectrum of relaxation times at the plateau onset time of the mean square displacement vs time curves. In addition, from these curves, $G'(\omega)$ and $G''(\omega)$ were calculated for the WM solutions in a wide range of frequencies. This DWS microrheological information allowed us to estimate the characteristic lengths of the WM network; namely, the mesh size, the entanglement length, the persistence length, and the contour length for micellar solutions of different surfactant composition, surfactant ratio (R= [SDS]/[TDPS]), temperature, and salt concentration. The contour length is strongly modified with salt addition. When the brine concentration reaches a salt concentration of 0.225 M, where the electrostatic charges in the WMs are totally screened, the contour length can reach up to 12 μm, at T = 20 °C. When more salt is added to the system, the scission energy of the micelles decreases, and as a consequence, the micelles become shorter.

Acknowledgment. Funds from SEP-CONACYT (81081) and DGAPA-UNAM (112508) are gratefully acknowledged. We acknowledge the technical help of C. Garza and S. Ramos.

References and Notes

(1) Dan, N.; Safran, S. A. *Adv. Colloid Interface Sci.* **2006**, *123−126*, 323.
(2) Zilman, A.; Safran, S. A.; Sottmann, T.; Strey, R. *Langmuir* **2004**, *20*, 2199.
(3) Wang, Z.; Larson, R. G. J. *Phys. Chem. B* **2009**, *113*, 13697.
(4) Appel, J.; Porte, G.; Khatory, A.; Kern, F.; Candau, S. J. *J. Phys. II France* **1992**, *2*, 1045.
(5) Candau, S. J.; Khatory, A.; Lequeux, F.; Kern, F. *J. Phys. IV, C1* **1993**, *3*, 197.
(6) Porte, G.; Gomati, R.; Haitamy, O.; Appell, L.; Marignan, J. *J. Phys. Chem.* **1986**, *90*, 5746.
(7) Cates, M. E. *Macromolecules* **1987**, *20*, 2289.
(8) Zana, R.; Kaler, E. W. *Giant Micelles: Properties and Applications*; CRC Press: Boca Raton, FL, 2007.
(9) Walker, L. M. *Curr. Opin. Colloid Interface Sci.* **2001**, *6*, 451.
(10) Ezrabi, S.; Tuval, E.; Aserin, A. *Adv. Colloid Interface Sci.* **2006**, *128−130*, 77.
(11) Dreiss, C. A. *Soft Matter* **2007**, *3*, 956.
(12) Berret, J. F. Rheology of Wormlike Micelles: Equilibrium Properties and Shear Banding Transitions. In Weiss, R. G., Terech, P. Eds.; *Molecular Gels. Materials with Self-Assembled Fibrillar Networks*; Springer: The Netherlands, 2006, p 663.
(13) MacKintosh, F. C.; Schmidt, C. F. *Curr. Opin. Colloid Interface Sci.* **1999**, *4*, 300.
(14) Squires, T. D.; Mason, T. G. *Annu. Rev. Fluid Mech.* **2010**, *42*, 413.
(15) Waigh, T. A. *Rep. Prog. Phys.* **2005**, *68*, 685.
(16) Mason, T. G.; Weitz, D. A. *Phys. Rev. Lett.* **1995**, *74*, 1250.
(17) Gisler, T.; Weitz, D. A. *Curr. Opin. Colloid Interface Sci.* **1998**, *3*, 586.
(18) Mukhopadhyay, A.; Granick, S. *Curr. Opin. Colloid Interface Sci.* **2001**, *6*, 423.
(19) Chen, D. T.; Weeks, E. R.; Crocker, J. C.; Islam, M. F.; Verna, R.; Gruber, J.; Levine, A. J.; Lubensky, T. C.; Yodh, A. G. *Phys. Rev. Lett.* **2003**, *90*, 108301.
(20) Maret, G.; Wolf, P. E. *Z. Phys. B* **1987**, *65*, 409.
(21) Pine, D. J.; Weitz, D. A.; Chaikin, P. M.; Herbolzheimer, E. *Phys. Rev. Lett.* **1988**, *60*, 1134.
(22) Harden, J. L.; Viasnoff, V. *Curr. Opin. Colloid Interface Sci.* **2001**, *6*, 438.
(23) van Zanten, J. H.; Rufener, K. P. *Phys. Rev. E* **2000**, *62*, 5389.
(24) Cardinaux, F.; Cipelleti, L.; Scheffold, F.; Schurtenberger, P. *Europhys. Lett.* **2002**, *57*, 738.
(25) Bellour, M.; Skouri, M.; Munch, J.-P.; Hébraud, P. *Eur. Phys. J. E* **2002**, *8*, 431.
(26) Galvan-Miyoshi, J.; Delgado, J.; Castillo, R. *Eur. Phys. J. E* **2008**, *26*, 369.
(27) Willenbacher, N.; Oelschlaeger, C.; Schopferer, M.; Fischer, P.; Cardinaux, F.; Scheffold, F. *Phys. Rev. Lett.* **2007**, *99*, 068302.
(28) Oelschlaeger, C.; Schopferer, M.; Scheffold, F.; Willenbacher, N. *Langmuir* **2009**, *25*, 716.
(29) Oelschlaeger, C.; Suwita, P.; Willenbacher, N. *Langmuir* **2010**, *26*, 7045.
(30) Hoffmannm, H.; Rauscher, A.; Gradzielski, M.; Schulz, S. F. *Langmuir* **1992**, *8*, 2140.
(31) Lopez-Diaz, D.; Garcia-Mateos, I.; Velazquez, M. M. *Colloids Surf. A* **2005**, *270, 271*, 153.
(32) Pimenta, P.; Pashkovski, E. E. *Langmuir* **2006**, *22*, 3980.
(33) Lopez-Diaz, D.; Sarmiento-Gomez, E.; Garza, C.; Castillo, R. *J. Colloid Interface Sci.* **2010**, *348*, 152.
(34) Lopez-Diaz, D.; Castillo, R. *J. Phys. Chem. B* **2010**, *114*, 8917.
(35) Dasgupta, B. R.; Tee, S. Y.; Crocker, J. C.; Frisken, B. J.; Weitz, D. A. *Phys. Rev. E* **2002**, *65*, 51505.
(36) Galvan-Miyoshi, J.; Castillo, R. *Rev. Mex. Fis.* **2008**, *54*, 257.
(37) Rojas-Ochoa, L. F.; Lacoste, D.; Lenke, R.; Schurtenberger, P.; Scheffold, F. *J. Opt. Soc. Am. A* **2004**, *21*, 1799.
(38) Ishimaru, A. *Wave Propagation and Scattering in Random Media*; Academic Press: New York, 1978.
(39) van de Hulst, H. C. *Light Scattering by Small Particles*; Dover: New York, 1981.
(40) Kern, F.; Zana, R.; Candau, S. J. *Langmuir* **1991**, *7*, 1344.
(41) Doi, M.; Edwards, S. F. *The Theory of Polymer Dynamics*; Claredon: Oxford, 1986.
(42) Granek, R.; Cates, M. E. *J. Chem. Phys.* **1992**, *96*, 4758.
(43) Nettesheim, F.; Wagner, N. J. *Langmuir* **2007**, *23*, 5267.
(44) Shikata, R.; Dahman, S. J.; Pearson, D. S. *Langmuir* **1994**, *10*, 3470.
(45) Schubert, B. A.; Kaler, E. W.; Wagner, N. J. *Langmuir* **2003**, *19*, 4079.
(46) Kern, F.; Lequeux, F.; Zana, R.; Candau, S. J. *Langmuir* **1994**, *10*, 1714.
(47) Shikata, T.; Hirata, H.; Kotaka, T. *Langmuir* **1987**, *3*, 1081.

(48) Raghavan, S. R.; Fritz, G.; Kaler, E. W. *Langmuir* **2002**, *18*, 3797.
(49) Sharma, S. C.; Shrestha, R. G.; Shrestha, L. K.; Aramaki, K. *J. Phys. Chem. B* **2009**, *113*, 1615.
(50) Lequeux, F. *Europhys. Lett.* **1992**, *8*, 675.
(51) MacKintosh, F. C.; Safran, S. A.; Pincus, P. A. *Europhys. Lett.* **1990**, *12*, 697.
(52) Safran, S. A.; Pincus, P. A.; Cates, M. E.; MacKintosh, F. C. *J. Phys. (Paris)* **1990**, *51*, 503.
(53) Bellour, M.; Knaebel, A.; Munch, J. P.; Candau, S. J. *Eur. Phys. J. E* **2000**, *3*, 111.
(54) Bulut, S. J.; Hamit, J.; Olsson, U.; Kato, T. *Eur. Phys. J. E* **2008**, *27*, 261.
(55) Schurtenberger, P.; Cavaco, C.; Tiberg, F.; Regev, O. *Langmuir* **1996**, *12*, 2894 .

JP104996H